Journal of Controlled Release 231 (2016) 77–85

Contents lists available at ScienceDirect

Journal of Controlled Release

journal homepage: www.elsevier.com/locate/jconrel

Sonoporation enhances liposome accumulation and penetration in tumors with low EPR

Benjamin Theek [a], Maike Baues [a], Tarun Ojha [a], Diana Möckel [a], Seena Koyadan Veettil [b], Julia Steitz [b], Louis van Bloois [c], Gert Storm [c,d], Fabian Kiessling [a,*], Twan Lammers [a,c,d,*]

[a] Department of Experimental Molecular Imaging, University Clinic and Helmholtz Institute for Biomedical Engineering, RWTH-Aachen University, Aachen, Germany
[b] Institute for Laboratory Animal Science, University Clinic, RWTH-Aachen University, Aachen, Germany
[c] Department of Pharmaceutics, Utrecht Institute for Pharmaceutical Sciences, Utrecht University, Utrecht, The Netherlands
[d] Department of Targeted Therapeutics, MIRA Institute for Biomedical Technology and Technical Medicine, University of Twente, Enschede, The Netherlands

ARTICLE INFO

Article history:
Received 1 December 2015
Received in revised form 4 February 2016
Accepted 10 February 2016
Available online 12 February 2016

Keywords:
Sonoporation
Microbubbles
Ultrasound
EPR
Liposomes

ABSTRACT

The Enhanced Permeability and Retention (EPR) effect is a highly variable phenomenon. To enhance EPR-mediated passive drug targeting to tumors, several different pharmacological and physical strategies have been evaluated over the years, including e.g. TNFα-treatment, vascular normalization, hyperthermia and radiotherapy. Here, we systematically investigated the impact of sonoporation, i.e. the combination of ultrasound (US) and microbubbles (MB), on the tumor accumulation and penetration of liposomes. Two different MB formulations were employed, and their ability to enhance liposome accumulation and penetration was evaluated in two different tumor models, which are both characterized by relatively low levels of EPR (i.e. highly cellular A431 epidermoid xenografts and highly stromal BxPC-3 pancreatic carcinoma xenografts). The liposomes were labeled with two different fluorophores, enabling in vivo computed tomography/fluorescence molecular tomography (CT-FMT) and ex vivo two-photon laser scanning microscopy (TPLSM). In both models, in spite of relatively high inter- and intra-individual variability, a trend towards improved liposome accumulation and penetration was observed. In treated tumors, liposome concentrations were up to twice as high as in untreated tumors, and sonoporation enhanced the ability of liposomes to extravasate out of the blood vessels into the tumor interstitium. These findings indicate that sonoporation may be a useful strategy for improving drug targeting to tumors with low EPR.

1. Introduction

In nanomedicine, carrier materials with a size of 1–100(0) nm are employed to improve the biodistribution of systemically administered (chemo-) therapeutic drugs. Upon i.v. injection, nanocarrier materials such as liposomes, polymers and micelles circulate for prolonged periods of time, and via the Enhanced Permeability and Retention (EPR) effect, they gradually accumulate at pathological sites [1,2]. EPR is based on the notion that blood vessels in tumors (and at sites of inflammation) are leaky, while functional lymphatic drainage is absent, together leading to a relatively effective and selective target site localization. An additional important advantage of using nanomedicine formulations is that they, because of their relatively large size, prevent drug molecules from accumulating in healthy tissues. Clinically, most progress in the nanomedicine field has thus far been made by the latter, i.e. by "site-avoidance drug delivery", resulting in treatments which are less toxic and better tolerated by patients [3,4]. One of the key challenges for the nanomedicine field for the next couple of years will be to demonstrate – at the clinical level – that carrier materials can also be employed for "site-specific drug delivery", and as such are able to really improve response rates and survival times in patients.

In this context, one has to bear in mind that the somewhat disappointing results that have been obtained thus far are only partially due to the nanomedicine formulations themselves. It is more and more recognized that EPR is a highly variable phenomenon, both in animal models and in patients, and even within a single patient and within a single tumor, some vessels are more leaky than others [5–8]. Potential reasons for this high variability are manifold, including e.g. differences in the relative blood volume in tumors, in tumor blood flow, in vascular permeability, in stromal content, in cellularity and in the interstitial fluid pressure (IFP) [6,9–12]. Consequently, besides on making ever more nanocarrier materials, we should also focus on developing

* Corresponding authors at: Department of Experimental Molecular Imaging, University Clinic and Helmholtz Institute for Biomedical Engineering, RWTH-Aachen University, Aachen, Germany.
E-mail addresses: fkiessling@ukaachen.de (F. Kiessling), tlammers@ukaachen.de (T. Lammers).

http://dx.doi.org/10.1016/j.jconrel.2016.02.021
0168-3659/

strategies to overcome this high variability in EPR, and on methods to monitor and modulate EPR, in order to increase the chances of clinical success.

The most straightforward strategy in this regard is to use imaging to pre-select patients, as patients presenting with sufficiently high levels of EPR in tumors (and metastases) are more likely to show good therapeutic responses upon nanomedicine treatment than patients with low or no EPR [7,10,13–15]. A potential shortcoming of this is that non-invasive imaging of EPR-mediated drug targeting (which is routinely performed using radiolabeled nanocarriers and nuclear medicine techniques such as gamma-scintigraphy, PET or SPECT) only reports on the overall levels of tumor accumulation, and not on their penetration and intratumoral distribution. It seems likely, however, that the overall amount of nanocarrier accumulation – which is generally expressed as percent of the injected dose per gram or kilogram of tumor tissue – is not the only parameter determining therapeutic efficacy, and that also an efficient penetration deep into the tumor interstitium is needed to allow for potent antitumor responses [16].

Since many tumors, and in particular tumors in patients, present with an extensive stromal compartment, characterized e.g. by a tight perivascular cell coverage and by a dense collagen network, the penetration of drugs and drug delivery systems into the tumor interstitium is limited, and their intratumoral distribution is suboptimal [3,17–21]. In the last 1–2 decades, several strategies have been evaluated to enhance extravasation and penetration, based primarily on pharmacological and physical co-treatments. Pharmacological modulation e.g. refers to the co-administration of inflammatory mediators (such as TNF-α), agents inducing hypertension (such as angiotensin) and agents inducing vascular normalization (such as bevacizumab) [22–26]. Physical co-treatments include hyperthermia, radiotherapy and sonoporation [9,27–29].

In recent years, sonoporation, which is based on the combination of ultrasound (US) and microbubbles (MB), has been receiving ever more attention [28–33]. Via stable and inertial cavitation effects, such as microstreaming, jet formation and shock waves, cell membranes can be permeabilized and tight junctions in vascular endothelium can be opened. Thus far, sonoporation has been primarily used for nucleic acid delivery across the membrane of (cancer) cells, which works well, especially in vitro. In vivo, one has to keep in mind that MB are exclusively confined to the vascular compartment, as they are too large to extravasate. Consequently, the main in vivo applications of MB and sonoporation are within the vasculature, encompassing e.g. the lysis of blood clots and the permeation of the blood–brain barrier (BBB) [34–36]. The latter application is particularly attractive, as the BBB prevents the majority of drug molecules from entering the brain, and as there are hardly any other means to enable efficient drug delivery across the BBB. Aiming to enhance drug delivery to brain tumors, McDannold and colleagues showed that doxorubicin concentrations in 9 L gliomas in rats can be doubled when liposomal doxorubicin is co-administered with MB and focused US [36]. Beyond the brain and brain tumors, hardly any studies are available showing that sonoporation can be employed to improve drug delivery to tumors. In the majority of these cases, the MB themselves were used as drug delivery devices [37–41], and apart from a single study by Lin et al., in which sonoporation was combined with liposomal doxorubicin, and in which increases in drug concentrations of up to 30% were achieved [42], no studies have analyzed the impact of sonoporation on the tumor accumulation and penetration of nanomedicine formulations.

Here, we therefore systematically analyzed the impact of sonoporation on the tumor accumulation and penetration of fluorophore-labeled liposomes. This was done using two different types MB formulations (i.e. phospholipid-based soft-shell MB and polymer-based hard-shell MB), whose oscillation potential differs due to their different shell stiffness, and two different tumor models (i.e. highly cellular A431 epidermoid tumors and highly stromal BxPC-3 tumors), which are both characterized by low levels of EPR. The overall tumor accumulation of the liposomes was monitored using hybrid computed tomography/fluorescence molecular tomography (CT-FMT) [43,44], and their penetration out of the blood vessels into the tumor interstitium was visualized and quantified using two-photon laser scanning microscopy (TPLSM) [45]. Our findings show that sonoporation can be used to enhance both the macro-accumulation and the micro-distribution of liposomal nanocarriers in tumors, and they indicate that sonoporation might be an interesting method to improve the efficacy of nanomedicine treatments in tumors with low levels of EPR.

2. Materials & methods

2.1. Materials

Sodium bicarbonate, cholesterol and Triton X-100 were purchased from Sigma-Aldrich, USA. DPPC was obtained from Lipoid, Germany, and PEG(2000)-DSPE-NH_2 and PEG(2000)-DSPE from Avanti Polar Lipids, USA. NBD-PE, which fluoresces at 488 nm, was obtained from Molecular Probes, USA. The near-infrared fluorescent dye Alexa Fluor 750 NHS ester was purchased from Invitrogen, USA. n-Butyl cyanoacrylate was purchased from Special Polymer Ltd., Bulgaria. MicroMarker MB were ordered from Fujifilm Sonosite, The Netherlands.

2.2. Liposome synthesis

Green fluorescent liposomes were synthesized as described previously [45]. The near-infrared label was introduced by a post-insertion method using Alexa Fluor 750 labeled PEG-PE micelles. PEG-PE micelles were prepared by mixing 4 μmol PEG(2000)-DSPE-NH_2 and 4 μmol PEG(2000)-DSPE with 0.5 ml of a 0.1 M sodium bicarbonate solution at pH 8.3. This mixture was heated at 60 °C for 10 min. One milligram of Alexa Fluor 750 NHS ester was added to the 0.5 ml of PEG-PE micelles and covalently attached to the micelles by heating the solution at 60 °C for 10 min, and thereafter continuously mixed for 60 min at room temperature. During incubation and conjugation, PEG(2000)-DSPE-NH_2 was used in five-fold excess as compared to Alexa Fluor 750. Subsequently, Alexa Fluor 750 labeled PEG-PE micelles were added to the liposomes and heated for 5 min at 60 °C, followed by 10 min of mixing at room temperature. Heating and mixing were repeated 3 times. The liposomes were then extruded through polycarbonate filters for obtaining the desired diameter of 133 nm and a PDI of 0.04.

2.3. Microbubble synthesis

Poly(butyl cyanoacrylate) (PBCA)-based microbubbles were synthesized as described in [46]. In short, the n-Butyl cyanoacrylate monomer was added drop-wise to an aqueous solution containing 1% (w/v) TritonX-100 at pH 2.5, under mild mixing using an Ultra-turrax (IKA-Werke, Germany). Upon complete addition of the monomer, the mixture was stirred at 10,000 rpm for 60 min. Following the synthesis, several washing and purification steps were performed to obtain PBCA MB. Phospholipid-based MicroMarker MB were obtained from Fujifilm Sonosite (The Netherlands). Both MB formulations have an average size of 2 to 2.5 μm and a relatively broad size distribution, roughly ranging from 1.5–3 μm for PBCA-based polymeric MB and from 1 to 6 μm for commercial phospholipid-based MB.

2.4. Animal experiments

All animal experiments were performed according to the regulations of local and national committees for animal welfare (AZ 87-51.04.2010.A278). Six to eight week old female CD-1 nude mice were ordered from Charles River (The Netherlands) and kept in cages with food and water ad-libitum, separate ventilation and controlled light–dark cycles. Four million A431 cells (i.e. human epidermoid) or five million BxPC-3 cells (i.e. human pancreatic adenocarcinoma) were

inoculated subcutaneously into both flanks of the mice, and tumors were allowed to grow to 6–8 mm in diameter. Three days before the start of the sonoporation experiment, the diet was changed to chlorophyll-free food (ssniff Spezialdiäten GmbH, Germany), to reduce background fluorescence in the FMT analyses.

2.5. Ultrasound sonoporation

All in vivo ultrasound (US) experiments were conducted under continuous inhalation anesthesia, using 2% (vol/vol) isoflurane. The US device employed in this study was the VisualSonics Vevo2100 imaging system (Fujifilm Sonosite, The Netherlands). For sonoporation experiments, mice were placed onto the US table and a tail vein catheter was inserted for liposome and MB injection. Directly after liposome injection, $5 * 10^8$ MB were administered. After an i.v. bolus injection, the MB were continuously destroyed in the tumor (by moving the transducer linearly over the volume of interest) using Power Doppler US (fz = 16 MHz; MI = 0.9) for 10 min. The tumor accumulation of liposomes was imaged by CT-FMT hybrid imaging, as detailed below.

2.6. Hybrid CT-FMT and FRI measurements

Hybrid computed tomography–fluorescence molecular tomography (CT-FMT) and fluorescence reflectance imaging (FRI) analyses were performed as described in [47,48]. Briefly, anesthetized mice were placed into a custom-made mouse bed enabling both CT (CT Imaging, Germany) and FMT (PerkinElmer, USA) imaging. CT scans acquiring 720 projections in 1.1 full rotations on a flat panel detector with the size of 1032 × 1012 pixels were obtained. Mice were then transferred to the FMT and FRI device, in order to assess the tumor accumulation and the biodistribution of the fluorescent liposomes. To this end, a total of 100–120 FMT scan points, lying on a grid with a inter-individual distance of 3 mm were acquired from top and bottom view of the mice. This procedure was performed at 4, 24 and 48 h after the i.v. injection of the liposomes, in order to monitor (the effect of sonoporation on) their tumor accumulation longitudinally. After the last measurement, mice were i.v. injected with rhodamine-lectin (to stain functional blood vessels and facilitate microscopy analyses) and sacrificed 10 min later. Tumors were excised and imaged ex vivo, in fluorescence reflectance mode at 750 nm, to obtain a high-resolution image of liposome distribution near the surface. Afterwards, they were embedded in TissueTek O.C.T. (Sakura Finetek Europe, The Netherlands) for cryopreservation at −80 °C until further analysis. The CT and FMT data sets were reconstructed and fused. The hybrid CT-FMT data sets were analyzed using Imalytics Preclinical (GremseIT, Germany). Tumor segmentation was based on the anatomical information obtained by CT and dilated by 10 voxels to account for the lower spatial resolution of the reconstructed FMT data. The FMT-based biodistribution data was loaded as an overlay, and the fluorescence signal allocated to the tumor was quantified and expressed as % of the injected dose (%ID) per 250 mm^3 tumor. The relative increase in liposome accumulation was calculated by dividing the calculated %ID/250 mm^3 of sonoporated and contralateral control tumor. The 2D FRI images were normalized, with respect to LED power and exposure time, and analyzed using MATLAB R2015A (MathWorks, Natick, USA). The probability density plots are based on the combination of all five tumors per group.

2.7. Two-photon laser scanning microscopy

One hundred μm-thick sections were freshly prepared from the cryopreserved tumors before image acquisition. Image stacks of 50 images with a step size of 1 μm were acquired using a 25× water-immersed objective mounted on the Olympus FV1000MPE multiphoton microscopy system. In each image stack, fluorescent liposomes as well as perfused blood vessels (via rhodamine-lectin staining) and collagen content (via second-harmonic generation imaging) were imaged. Two-photon Laser Scanning Microscopy (TPLSM) images were analyzed using Imaris Software, Version 7.4 (Bitplane AG, Zurich, Switzerland). By means of intensity thresholding, the relative collagen content of the individual tumors was quantified. The micro-distribution of the NBD-containing fluorescent liposomes, i.e. their extravasation from blood vessels into the tumor interstitium, was analyzed using a modified version of the "Dilate Surface" XTension in Imaris. For this purpose, initially, thresholding was applied on the basis of the rhodamine-lectin signal, to create a 3D vessel segmentation, and on the NBD signal, to determine the volume of liposome distribution. The vessel segmentation was then automatically dilated, at step-sizes of 10 μm, 30 μm and 50 μm. Finally, the total amount of liposomes found within a 50 μm radius around the vessels was quantified by multiplying the relative liposome volume and signal intensity. The relative micro-distribution of liposomes was calculated, by determining the relative amount of liposomes found in each individual 3D segmentation, to compare the distribution of the liposomes in control and sonoporated tumors.

2.8. Immunohistochemistry

For immunohistochemistry (IHC), cryopreserved tumors were cut into 8 μm-thick sections and stored at −80 °C until further use. To determine the cellularity of the A431 and BxPC-3 tumors, DAPI stainings were performed. This was done by mixing DAPI with Mowiol (1:10) and by subsequently applying this to the tissue sections before covering them with a glass slide. Images were acquired using the AxioImager M2 microscopy system (Carl Zeiss AG, Jena, Germany), and cellularity was quantified by thresholding of the area fraction of DAPI per image using ImageJ. Three different fields-of-view (FOV) were quantified per section, three different sections per tumor, and five different tumors for each animal model. The results obtained from the five different tumors were averaged and analyzed for statistical significance.

2.9. Statistical analysis

Statistical analysis was performed using GraphPad Prism 5. In vivo CT-FMT analysis on liposome accumulation was analyzed using the paired t-test and two-way ANOVA. Ex vivo 2D-FRI measurements were analyzed using a paired t-test and corrected for multiple comparisons (Bonferroni). TPLSM and immunohistochemistry analysis were performed using unpaired t-tests. P-values of less than 0.05 were considered to be statistically significant.

3. Results & discussion

To improve drug targeting to tumors characterized by low levels of EPR, we here systematically analyzed the effect of sonoporation on the accumulation and penetration of liposomes. This was done in two different tumor models, using two different microbubble formulations and using double-fluorophore-labeled liposomes (see Fig. 1). The double-labeling strategy was employed to enable non-invasive and quantitative in vivo optical imaging of the macro-accumulation of the liposomes in tumors (making use of the optical window of tissues, which is optimal for dyes with an absorption wavelength beyond ~650 nm; [49,50]), and to at the same time enable ex vivo two-photon scanning microscopy (TPLSM), providing information on the penetration and the micro-distribution of the liposomes in tumors (note that for TPLSM, absorption wavelengths should be below <600 nm; [45]).

3.1. Effect of sonoporation on the in vivo accumulation of liposomes in tumors

To investigate the impact of sonoporation on the tumor accumulation of liposomes, hybrid 3D CT-FMT imaging was performed [44,48,51]. The quantification of the tumor accumulation of the double-

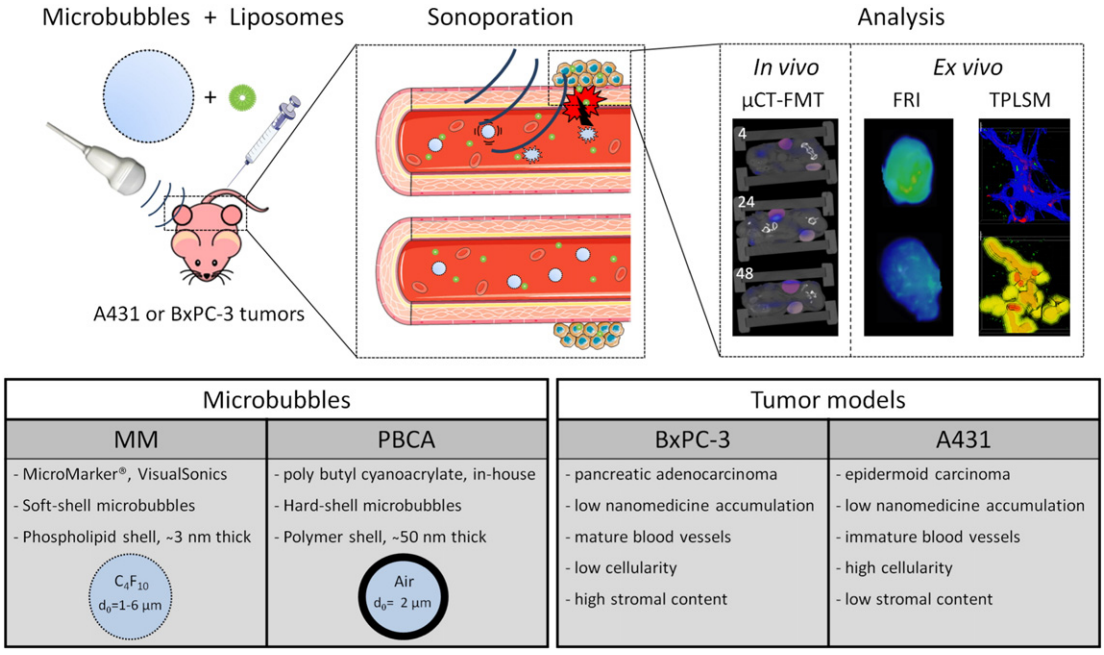

Fig. 1. Study design. Mice bearing A431 and BxPC-3 tumors on both flanks were co-injected with microbubbles and fluorophore-labeled liposomes. Microbubbles were locally destroyed in tumors on the right flank of mice, by exposing them to Power Doppler ultrasound pulses for 10 min. In vivo hybrid computed tomography - fluorescence molecular tomography (CT-FMT) was performed at 4, 24 and 48 h after i.v. injection, to visualize and quantify overall levels of liposome accumulation in tumors, and ex vivo fluorescence reflectance imaging (FRI) and two-photon laser scanning microscopy (TPLSM) were performed to evaluate liposome penetration.

labeled liposomes was analyzed as exemplarily shown in Fig. 2A–B. A maximum accumulation of 2.3 and 1.9% of the injected dose (ID) was found per 250 mm^3 in sonoporated A431 and BxPC-3 tumors, respectively. Control A431 and BxPC-3 tumors presented with a lower tumor accumulation, i.e. 1.4 and 1.5% ID per 250 mm^3 tumor, respectively. The highest values, i.e. 2.3% ID and 1.9% ID per 250 mm^3 tumor, were observed in the A431 + PBCA and BxPC-3 + MM groups, at 24 h after sonoporation, respectively, and were significantly higher than in the respective control groups (each having 1.3% ID/250 mm^3; Fig. 2C, F; $p = 0.02$). The other two groups, i.e. A431 + MM and BxPC-3 + PBCA, did not show significant enhancement of liposome accumulation, but did show a tendency towards increased concentrations. Most likely, the relatively low number of animals per experimental group (i.e. $n = 5$) and variability in the baseline levels of liposomes accumulating in tumors caused these values not to be significant. Such a high variability in the baseline levels of EPR has also been observed in other studies evaluating physical means to improve passive tumor targeting (e.g. hyperthermia and radiotherapy [27,52–54]). To address this inter-individual variability, we also calculated the relative increase in liposome accumulation in sonoporated (right) vs. control (left) tumors for each individual mouse. As shown in Table 1, in these analyses, it was found that liposome accumulation indeed always increased upon sonoporation: 4 h after sonoporation, increases of up to 113 ± 54% and 57 ± 55% were observed for A431 and BxPC-3 tumors, respectively. These differences decreased over time, with at 48 h p.i., increases of 33 ± 65% and 17 ± 54%, respectively. These findings indicate that sonoporation does work, but is dependent on the baseline variability in EPR, on the tumor model used, and on the time point after liposome administration.

3.2. Effect of sonoporation on the ex vivo accumulation of liposomes in tumors

Next, we confirmed the effect of sonoporation on the tumor accumulation of liposomes ex vivo. To this end, 2D-FRI images of excised tumors were obtained, and they were analyzed for overall levels of tumor accumulation as well as for the homogeneity of liposome distribution. As shown in Fig. 3A, overall, the 2D-FRI data supports the positive effect of sonoporation on liposome accumulation. In both A431 groups as well as in the BxPC-3 + PBCA group, increases of 20–50% were observed upon sonoporation, at 48 h after the i.v. injection of the liposomes. The greater range seen in the four sonoporation groups (Fig. 3B), compared to their control counterparts, supports the notion of sonoporation being rather heterogeneous. Fig. 3A furthermore visualizes how variable the EPR effect and the effect of sonoporation were, with on average, 3–4 out of 5 tumors showing a clear enhancement upon sonoporation, whereas in the other tumor(s), the situation tended to be the other way around. As explained above, this is likely due to differences in the baseline levels of EPR in these tumors. These differences in EPR result, at least in part, from differences in tumor perfusion. It is important to keep in mind in this regard that tumor perfusion does not only affect EPR, but also the ability of MB and sonoporation to enhance EPR-mediated tumor accumulation, as a reduced perfusion will also reduce the number of MB entering a tumor, and being available for sonoporation [55,56]. To address the impact of sonoporation on nanocarrier distribution within tumors, we also used 2D-FRI to quantitatively assess the homo/heterogeneity of liposome accumulation in tumors. As shown by Fig. 3C-F, this was done using probability density plots, suggesting that in the majority of cases, the distribution of pixel intensities (which is proportional to the liposome concentrations) broadens upon sonoporation, as exemplified by a marked right-shift towards higher pixel intensities.

3.3. Characterization of A431 and BxPC-3 tumors

The above observations indicate that sonoporation can have a positive effect on the macro-accumulation and the macro-distribution of liposomes in tumors. However, as already alluded to in the introduction, also the micro-distribution and the penetration of liposomes out of the blood vessels into the tumor interstitium are highly important for efficient drug delivery and drug therapy. Thus far, relatively little attention has been paid to liposome penetration, and to the best of our knowledge, this has never been systematically analyzed upon sonoporation. Therefore, we established a protocol, based on the combination of two-photon laser scanning microscopy (TPLSM) and advanced

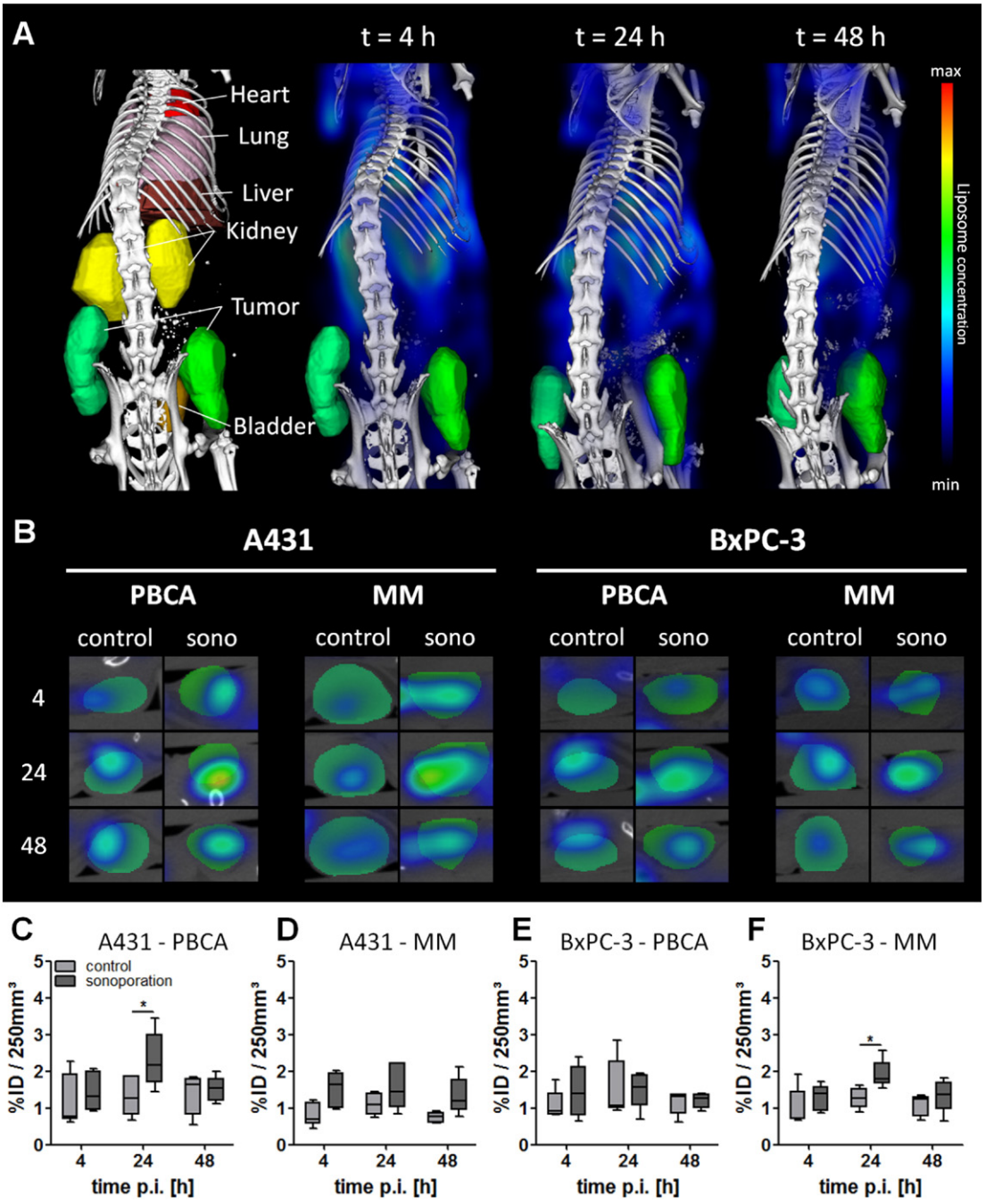

Fig. 2. In vivo tumor accumulation of liposomes. (A) Representative CT-FMT images of segmented organs and liposome distribution in mice. (B) Transversal slices through sonoporated (right) and control (left) tumors, indicating specific liposome accumulation. (C–F) Absolute liposome accumulation in A431 and BxPC-3 tumors upon sonoporation with PBCA and MM microbubbles over time, demonstrating a general tendency towards enhanced liposome accumulation upon sonoporation, but significant differences only in the A431 + PBCA and BxPC-3 + MM groups at 24 h p.i. The values represent average, 25/75 percentile (boxes) and minimum and maximum values (whiskers). * indicates $p < 0.05$.

Table 1
Relative increase in the overall tumor accumulation of liposomes upon sonoporation in A431 and BxPC-3 tumors. The effect of sonoporation was inter-individually corrected, by comparing liposome accumulation in untreated control tumors (left) with sonoporated tumors (right). Enhancement ratios were individually calculated for each mouse and are presented as an average value plus/minus standard deviation for each group.

Tumor model	A431		BxPC-3	
Microbubble type	PBCA	MM	PBCA	MM
4 h	+48 (±55) %	+113 (±54) %	+57 (±55) %	+56 (±50) %
24 h	+87 (±31) %	+63 (±60) %	+26 (±56) %	+54 (±22) %
48 h	+33 (±65) %	+90 (±51) %	+17 (±54) %	+33 (±40) %

image analysis, to evaluate the penetration of fluorophore-labeled nanocarriers in tumors. TPLSM and immunohistochemistry (IHC) analysis not only allowed to image liposomes and liposome penetration, but also provided information on the tumor microenvironment (i.e. relative blood volume, collagen content and cellularity).

We initially employed these techniques to characterize the two tumor models used. In this context, Fig. 4A–B show representative TPLSM (A) and IHC (B) images of A431 and BxPC-3 tumors, showing segmented vessels, collagen and nuclei. The vessel segmentation is based on the injection of fluorescently-labeled lectin, which stains functional blood vessels. A relatively low relative blood volume (rBV) of 1.8% (Fig. 4A, C) was detected for A431 tumors. Additionally, second

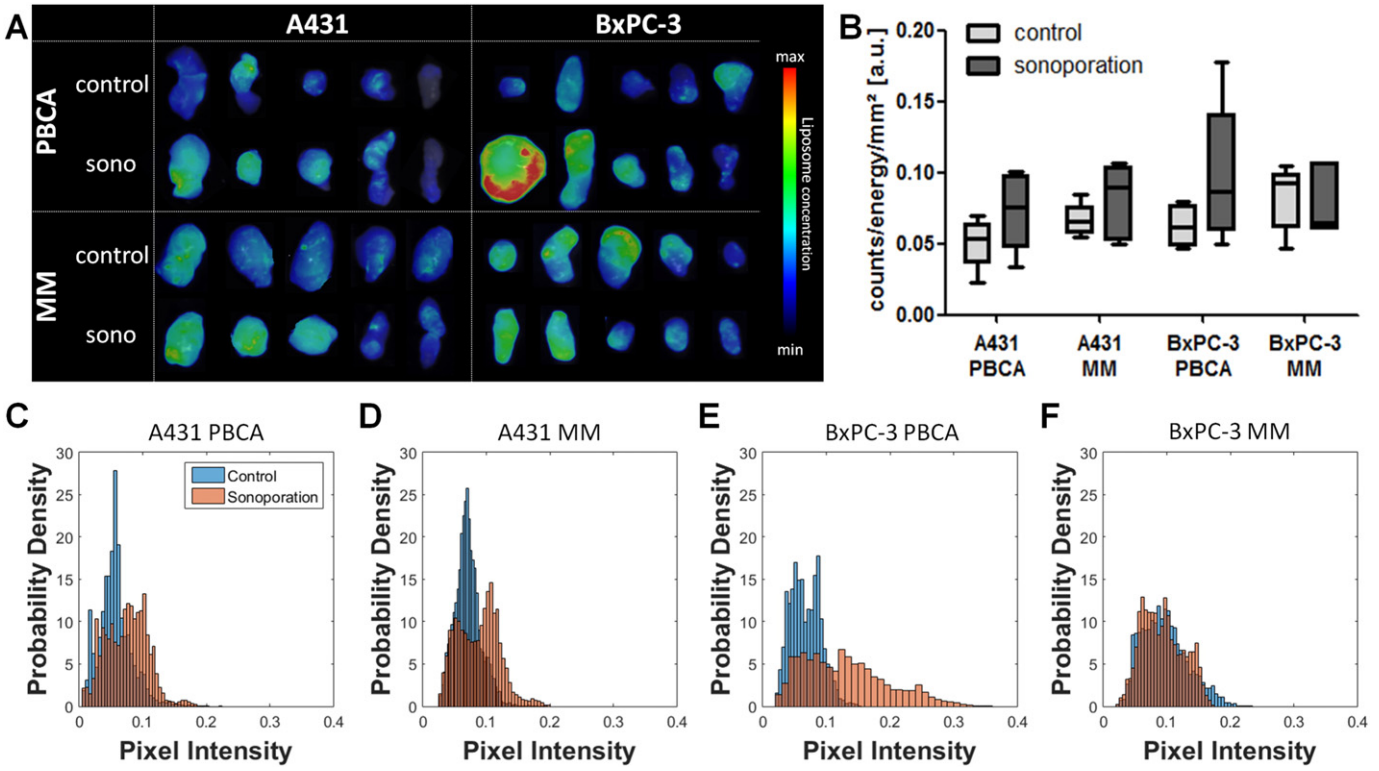

Fig. 3. Ex vivo tumor accumulation of liposomes. (A) 2D-FRI images of excised control and sonoporated A431 and BxPC-3 tumors, showing that in the majority of cases, sonoporation enhances liposome accumulation. (B) Quantification of mean signal intensity of fluorescent liposomes accumulating in the individual groups. (C–F) Probability density plots, showing an improvement in the homogeneity of liposome distribution in tumors upon sonoporation.

harmonic generation imaging revealed a collagen volume fraction of only 3% (Fig. 4D), of which half is found within the first 50 μm surrounding the blood vessels (Fig. 4E). DAPI staining and IHC furthermore revealed a very high cellularity (Fig. 4B, F). These findings are in line with the notion that A431 cells originate from an epidermoid tumor, where a dense cellular network and tight junctions govern the tumor structure. Furthermore it is known from literature that A431 tumors present many tiny and immature blood vessels [12]. Although such immature vessels are generally considered to be leaky, the very high cellular density and the limited intercellular space may explain why, in the absence of sonoporation, liposomes do not accumulate efficiently in A431 tumors. BxPC-3 tumors, on the other hand, originate from a stromal adenocarcinoma of the pancreas, and they present with much larger and much more mature vessels, characterized by much higher levels of pericyte coverage [21]. Their rBV is 2.7%, i.e. almost 50% higher than that of A431 tumors (Fig. 4A, C), and also their tumor

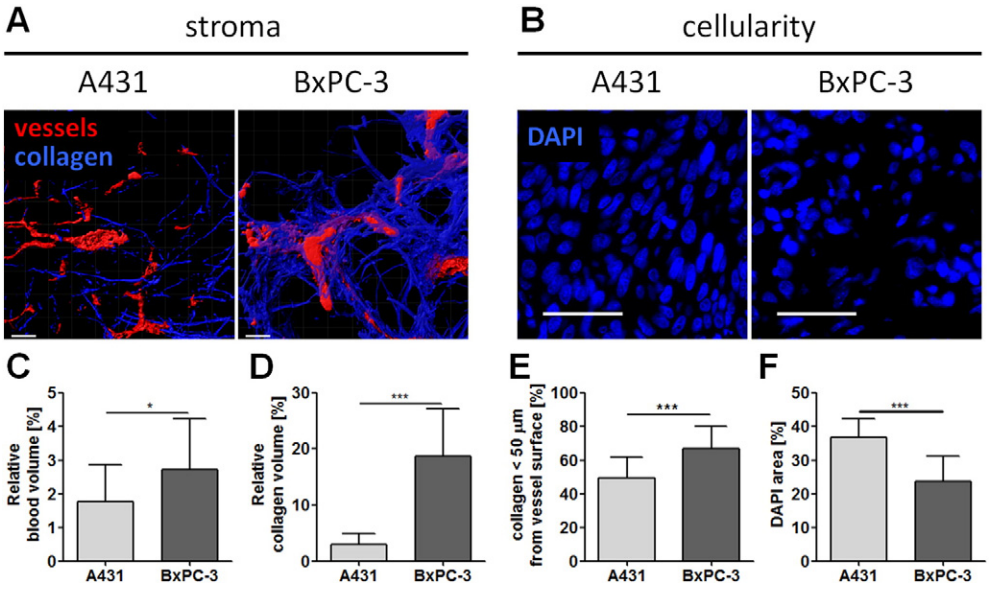

Fig. 4. TPLSM and IHC imaging of tumor and tumor stroma. Representative TPLSM images showing blood vessels (red) and collagen (blue) of A431 and BxPC-3 tumors (A). Corresponding quantification of the relative blood volume (C), the stromal collagen content (D) and distribution (E) revealed in significant differences in between both tumor models. DAPI staining of A431 and BxPC-3 tumors showing their cellularity in (B), revealed significantly higher values for A431 tumors (E). Size bars equal a distance of 50 μm.

microenvironment is very different, with more than 6 times more collagen present in the interstitium (Fig. 4A, D). Furthermore, in BxPC-3 tumors, blood vessels tend to be more closely associated with collagen than in A431 tumors (Fig. 4E). As it is well-known that a high collagen hinders the penetration of nanocarriers into tumors [17,57], in BxPB-3 tumors, the stromal compartment was considered to be the main factor limiting liposome accumulation and penetration, whereas in A431 tumors, poor EPR was mainly attributed to high cellularity. Keeping these phenotypic differences in mind, we next set out to evaluate the impact of sonoporation on liposome penetration in these two tumor models.

3.4. Effect of sonoporation on the penetration of liposomes in A431 and BxPC-3 tumors

To analyze the ability of sonoporation to enhance liposome penetration out of the blood vessels into the tumor interstitium, fluorescent signals within the first 50 μm of functional (i.e. lectin-positive) vessel were visualized and quantified. Liposome penetration was subdivided into three different fractions, i.e. less than 10 μm, 10–30 μm and 30–50 μm away from the vessel surface. As shown in Fig. 5A, C and D, in untreated A431 tumors, approximately two-thirds of the liposomes were found in direct vicinity to the vessel surface (67%), while the rest was distributed in the surrounding compartments. Upon sonoporation, the amount retained within the first 10 μm was found to be reduced, to 53% and 46%, upon sonoporation with PBCA and MM microbubbles, respectively. Correspondingly, in deeper areas within the tumors, higher amounts of liposomes were found upon sonoporation: in the 10–30 μm compartment, approximately 8% more liposomes were found in both groups after treatment, while in the 30–50 μm compartment, and enhancement of 4% and 12% was observed, for PBCA and MM, respectively.

In the collagen-rich BxPC-3 model, almost 80% of the liposomes clustered in the first 10 μm surrounding the blood vessel wall in the absence of sonoporation (Fig. 5B, E, F). This indicates that under control conditions, liposome penetration is worse in BxPC-3 tumors than in A431 tumors. Upon sonoporation, 18% and 15% less liposomes were detected in the first 10 μm surrounding the vessel wall, for PBCA and MM, respectively. In both MB groups, these reductions were found to be significant, indicating that sonoporation is a useful means to enhance the penetration of relatively large liposomal nanocarriers out of the blood vessels into the tumor interstitium. How sonoporation affects the accumulation and penetration of other drug delivery systems, e.g. of 5–10 nm-sized polymers, of 15–20 nm-sized antibodies, and of 30–50 nm-sized micelles, will be systematically studied in follow-up experiments.

In such analyses, it will be important to also address the mechanistic aspects of sonoporation, in order to better understand which

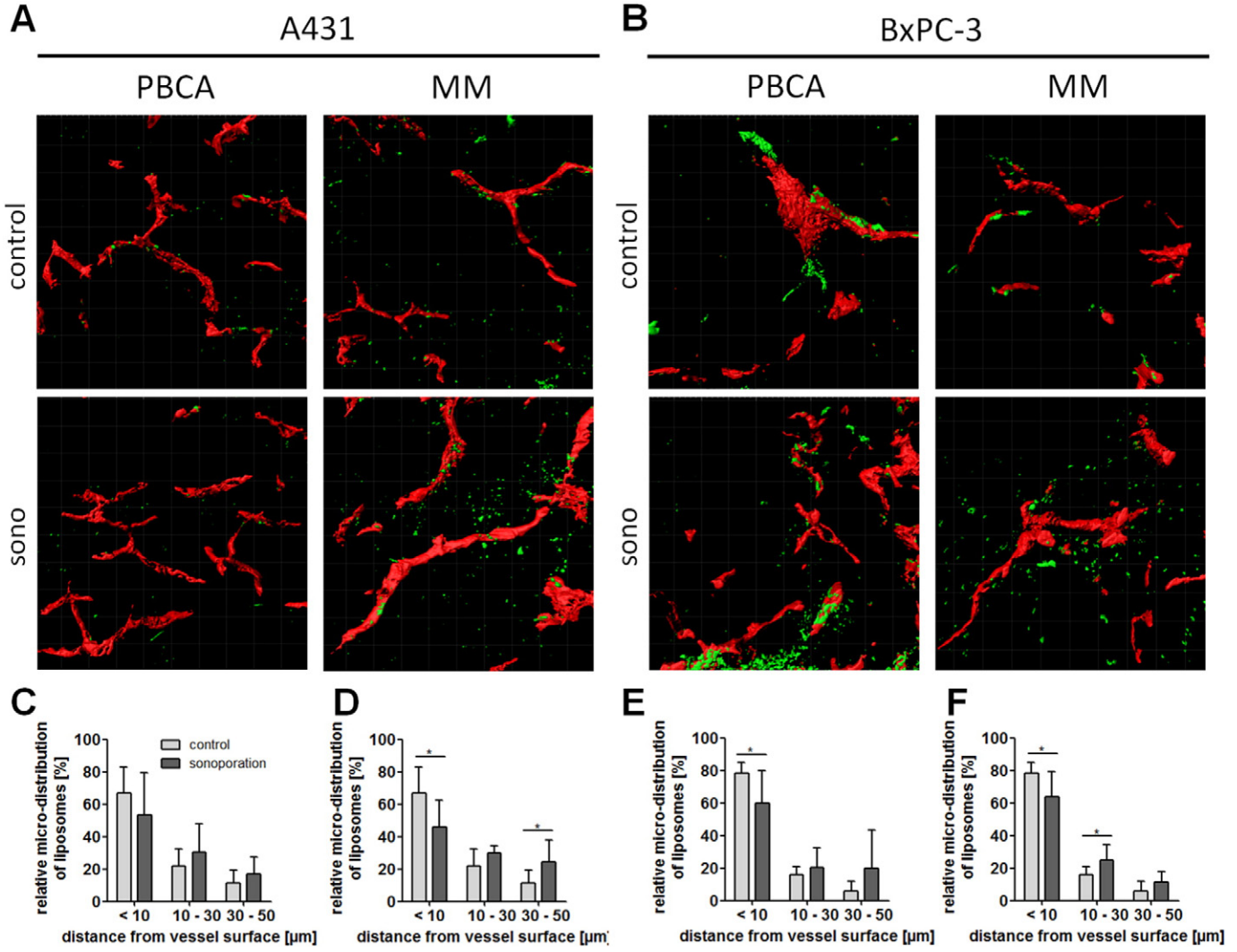

Fig. 5. Effect of sonoporation on the penetration of liposomes in A431 and BxPC-3 tumors. (A–B) Exemplary TPLSM images showing blood vessels (red) and liposomes (green) in control and sonoporated A431 and BxPC-3 tumors. (C–F) Relative distribution of liposomes in different tumor compartments upon sonoporation with PBCA (C, E) and MM (D, F) microbubbles. * Indicates $P < 0.05$.

sonoporation mechanism can be employed to permeate which type of blood vessel, and via which physiological effect. Several different sonoporation mechanisms, such as microstreaming, shockwave generation and jet formation, have been described, and it seems reasonable that depending on the sonoporation mechanism, several different physiological effects can be elicited, including e.g. enhanced perfusion of compressed blood vessels, loosening of tight junctions, endothelial pore formation, and modulation of the perivascular matrix [17,57]. These insights, including the differential mechanical and physical behavior of soft- vs. hard shell MB (for which we did not observe clear-cut differences in this study with regard to enhancement of liposome accumulation and penetration), will be addressed in future studies. Knowledge on such fundamental mechanism(s) of sonoporation is key to selecting the most optimal protocol for a given application. In this regard, one has to keep in mind that settings will likely be very different when e.g. intending to gently open up the blood–brain barrier for improved delivery of a low-molecular-weight drug, as compared to more rigorously opening up the endothelial lining and the perivascular matrix in tumors for enhanced nanomedicine accumulation and penetration.

Taking everything together, we here show that sonoporation, using both soft-shell and hard-shell MB, can be employed to enhance the accumulation and penetration of liposomes in tumors characterized by low levels of EPR. Differences of up to 100% were observed, but also a high inter- and intra-individual variability. Partially because of this high variability, sonoporation effects appeared to be independent of the MB formulation used and of the tumor model tested. These findings need to be verified and extended in future analyses, employing different US settings, different types of nanocarriers and different preclinical setups (e.g. permeation of blood vessels in brain vs. in tumor). The proof-of-principle findings reported here are considered to be important for furthering sonoporation efforts in the clinic, aiming to improve drug delivery to tumors and to the brain. Pioneering recent studies have shown in this regard that sonoporation can be employed to enhance the efficacy of gemcitabine-based chemotherapy in pancreatic cancer patients [58], and also to open up the blood–brain barrier for improved doxorubicin delivery to tumors in glioblastoma patients. This, together with systematic and mechanistic studies at the preclinical level, will help to create a solid framework for integrating sonoporation in drug delivery and drug therapy, especially in case of incurable and life-threatening cancers and neurodegenerative disorders.

4. Conclusion

Since the EPR effect is a highly variable phenomenon, and since many tumors do not present with sufficiently high levels of EPR to ensure proper tumor accumulation and antitumor efficacy, several different physical and pharmacological co-treatments are being evaluated to improve EPR-mediated tumor targeting. We here show that sonoporation can be used to enhance the accumulation and penetration of 100 nm-sized liposomes in tumors characterized by low levels of EPR. The positive effects of sonoporation depended on baseline variability in EPR, but consistently pointed towards improvements in both overall tumor concentration and intratumoral distribution. These findings support currently ongoing efforts to use sonoporation in the clinic, for improving drug delivery and drug therapy in pancreatic cancer and glioblastoma patients.

Acknowledgments

The authors gratefully acknowledge the financial support from the European Research Council (ERC-StG-309495-NeoNaNo), by the European Union (COST-Action-TD1004-Nanotheragnostics and H2020-ITN-642028-NABBA), by the DFG (LA 2937/1-2), by the Excellence Initiative of the German federal and State Governments in the framework of the i^{3}tm Seed Fund Program (SF_14-4-09-Sonoporation) and by the German Federal State of North Rhine Westphalia (HighTech.NRW/EU-Ziel 2-Programm (EFRE); ForSaTum). Furthermore, we would like to thank the IZKF two-photon imaging facility at RWTH Aachen University Clinic (Dr. Michael Vogt, Prof. Marc van Zandvoort) for the assistance with the TPLSM measurements.

References

[1] Y. Matsumura, H. Maeda, A new concept for macromolecular therapeutics in cancer chemotherapy: mechanism of tumoritropic accumulation of proteins and the antitumor agent SMANCS, Cancer Res. 46 (1986) 6387–6392.
[2] H. Maeda, Macromolecular therapeutics in cancer treatment: the EPR effect and beyond, J. Control. Release 164 (2012) 138–144.
[3] R.K. Jain, T. Stylianopoulos, Delivering nanomedicine to solid tumors, Nat. Rev. Clin. Oncol. 7 (2010) 653–664.
[4] T. Lammers, SMART drug delivery systems: back to the future vs. clinical reality, Int. J. Pharm. (2013).
[5] M.I. Koukourakis, S. Koukouraki, A. Giatromanolaki, S. Kakolyris, V. Georgoulias, A. Velidaki, S. Archimandritis, N.N. Karkavitsas, High intratumoral accumulation of stealth liposomal doxorubicin in sarcomas—rationale for combination with radiotherapy, Acta Oncol. 39 (2000) 207–211.
[6] K.J. Harrington, S. Mohammadtaghi, P.S. Uster, D. Glass, A.M. Peters, R.G. Vile, J.S. Stewart, Effective targeting of solid tumors in patients with locally advanced cancers by radiolabeled pegylated liposomes, Clin. Cancer Res. 7 (2001) 243–254.
[7] T. Lammers, L.Y. Rizzo, G. Storm, F. Kiessling, Personalized nanomedicine, Clin. Cancer Res. 18 (2012) 4889–4894.
[8] D. Simberg, Opening windows into tumors, ACS Nano (2015).
[9] T. Lammers, F. Kiessling, W.E. Hennink, G. Storm, Drug targeting to tumors: principles, pitfalls and (pre-) clinical progress, J. Control. Release 161 (2012) 175–187.
[10] L.Y. Rizzo, B. Theek, G. Storm, F. Kiessling, T. Lammers, Recent progress in nanomedicine: therapeutic, diagnostic and theranostic applications, Curr. Opin. Biotechnol. 24 (2013) 1159–1166.
[11] N. Bertrand, J. Wu, X. Xu, N. Kamaly, O.C. Farokhzad, Cancer nanotechnology: the impact of passive and active targeting in the era of modern cancer biology, Adv. Drug Deliv. Rev. 66 (2014) 2–25.
[12] J. Ehling, B. Theek, F. Gremse, S. Baetke, D. Mockel, J. Maynard, S.A. Ricketts, H. Grull, M. Neeman, R. Knuechel, W. Lederle, F. Kiessling, T. Lammers, Micro-CT imaging of tumor angiogenesis: quantitative measures describing micromorphology and vascularization, Am. J. Pathol. 184 (2014) 431–441.
[13] B. Theek, L.Y. Rizzo, J. Ehling, F. Kiessling, T. Lammers, The theranostic path to personalized nanomedicine, Clin. Transl. Imaging 2 (2014) 66–76.
[14] T. Ojha, L. Rizzo, G. Storm, F. Kiessling, T. Lammers, Image-guided drug delivery: preclinical applications and clinical translation, Expert Opin. Drug Deliv. (2015) 1–5.
[15] S. Kunjachan, J. Ehling, G. Storm, F. Kiessling, T. Lammers, Noninvasive imaging of nanomedicines and nanotheranostics: principles, progress, and prospects, Chem. Rev. 115 (2015) 10907–10937.
[16] L. Davies Cde, L.M. Lundstrom, J. Frengen, L. Eikenes, S.O. Bruland, O. Kaalhus, M.H. Hjelstuen, C. Brekken, Radiation improves the distribution and uptake of liposomal doxorubicin (caelyx) in human osteosarcoma xenografts, Cancer Res. 64 (2004) 547–553.
[17] P.A. Netti, D.A. Berk, M.A. Swartz, A.J. Grodzinsky, R.K. Jain, Role of extracellular matrix assembly in interstitial transport in solid tumors, Cancer Res. 60 (2000) 2497–2503.
[18] Z. Popovic, W. Liu, V.P. Chauhan, J. Lee, C. Wong, A.B. Greytak, N. Insin, D.G. Nocera, D. Fukumura, R.K. Jain, M.G. Bawendi, A nanoparticle size series for in vivo fluorescence imaging, Angew. Chem. Int. Ed. Engl. 49 (2010) 8649–8652.
[19] T. Stylianopoulos, B. Diop-Frimpong, L.L. Munn, R.K. Jain, Diffusion anisotropy in collagen gels and tumors: the effect of fiber network orientation, Biophys. J. 99 (2010) 3119–3128.
[20] C. Wong, T. Stylianopoulos, J. Cui, J. Martin, V.P. Chauhan, W. Jiang, Z. Popovic, R.K. Jain, M.G. Bawendi, D. Fukumura, Multistage nanoparticle delivery system for deep penetration into tumor tissue, Proc. Natl. Acad. Sci. U. S. A. 108 (2011) 2426–2431.
[21] H. Cabral, Y. Matsumoto, K. Mizuno, Q. Chen, M. Murakami, M. Kimura, Y. Terada, M.R. Kano, K. Miyazono, M. Uesaka, N. Nishiyama, K. Kataoka, Accumulation of sub-100 nm polymeric micelles in poorly permeable tumours depends on size, Nat. Nanotechnol. 6 (2011) 815–823.
[22] W. Cai, Z.J. Kerner, H. Hong, J. Sun, Targeted cancer therapy with tumor necrosis factor-alpha, Biochem. Insights 2008 (2008) 15–21.
[23] S. Goel, D.G. Duda, L. Xu, L.L. Munn, Y. Boucher, D. Fukumura, R.K. Jain, Normalization of the vasculature for treatment of cancer and other diseases, Physiol. Rev. 91 (2011) 1071–1121.
[24] V.P. Chauhan, T. Stylianopoulos, J.D. Martin, Z. Popovic, O. Chen, W.S. Kamoun, M.G. Bawendi, D. Fukumura, R.K. Jain, Normalization of tumour blood vessels improves the delivery of nanomedicines in a size-dependent manner, Nat. Nanotechnol. 7 (2012) 383–388.
[25] U. Prabhakar, H. Maeda, R.K. Jain, E.M. Sevick-Muraca, W. Zamboni, O.C. Farokhzad, S.T. Barry, A. Gabizon, P. Grodzinski, D.C. Blakey, Challenges and key considerations of the enhanced permeability and retention effect for nanomedicine drug delivery in oncology, Cancer Res. 73 (2013) 2412–2417.
[26] H. Nehoff, N.N. Parayath, L. Domanovitch, S. Taurin, K. Greish, Nanomedicine for drug targeting: strategies beyond the enhanced permeability and retention effect, Int. J. Nanomedicine 9 (2014) 2539–2555.

[27] G. Kong, M.W. Dewhirst, Hyperthermia and liposomes, Int. J. Hyperth. 15 (1999) 345–370.
[28] K. Kooiman, H.J. Vos, M. Versluis, N. de Jong, Acoustic behavior of microbubbles and implications for drug delivery, Adv. Drug Deliv. Rev. 72 (2014) 28–48.
[29] I. Lentacker, I. De Cock, R. Deckers, S.C. De Smedt, C.T. Moonen, Understanding ultrasound induced sonoporation: definitions and underlying mechanisms, Adv. Drug Deliv. Rev. 72 (2014) 49–64.
[30] R. Deckers, C.T. Moonen, Ultrasound triggered, image guided, local drug delivery, J. Control. Release 148 (2010) 25–33.
[31] S. Mo, C.C. Coussios, L. Seymour, R. Carlisle, Ultrasound-enhanced drug delivery for cancer, Expert Opin. Drug Deliv. 9 (2012) 1525–1538.
[32] F. Kiessling, S. Fokong, J. Bzyl, W. Lederle, M. Palmowski, T. Lammers, Recent advances in molecular, multimodal and theranostic ultrasound imaging, Adv. Drug Deliv. Rev. 72 (2014) 15–27.
[33] A.K. Wood, C.M. Sehgal, A review of low-intensity ultrasound for cancer therapy, Ultrasound Med. Biol. 41 (2015) 905–928.
[34] F. Kiessling, S. Fokong, P. Koczera, W. Lederle, T. Lammers, Ultrasound microbubbles for molecular diagnosis, therapy, and theranostics, J. Nucl. Med. 53 (2012) 345–348.
[35] T. Lammers, P. Koczera, S. Fokong, F. Gremse, J. Ehling, M. Vogt, A. Pich, G. Storm, M. van Zandvoort, F. Kiessling, Theranostic USPIO-loaded microbubbles for mediating and monitoring blood–brain barrier permeation, Adv. Funct. Mater. 25 (2015) 36–43.
[36] M. Aryal, J. Park, N. Vykhodtseva, Y.Z. Zhang, N. McDannold, Enhancement in blood-tumor barrier permeability and delivery of liposomal doxorubicin using focused ultrasound and microbubbles: evaluation during tumor progression in a rat glioma model, Phys. Med. Biol. 60 (2015) 2511–2527.
[37] J. Kang, X. Wu, Z. Wang, H. Ran, C. Xu, J. Wu, Z. Wang, Y. Zhang, Antitumor effect of docetaxel-loaded lipid microbubbles combined with ultrasound-targeted microbubble activation on VX2 rabbit liver tumors, J. Ultrasound Med. 29 (2010) 61–70.
[38] S. Tinkov, C. Coester, S. Serba, N.A. Geis, H.A. Katus, G. Winter, R. Bekeredjian, New doxorubicin-loaded phospholipid microbubbles for targeted tumor therapy: in-vivo characterization, J. Control. Release 148 (2010) 368–372.
[39] M.C. Cochran, J.R. Eisenbrey, M.C. Soulen, S.M. Schultz, R.O. Ouma, S.B. White, E.E. Furth, M.A. Wheatley, Disposition of ultrasound sensitive polymeric drug carrier in a rat hepatocellular carcinoma model, Acad. Radiol. 18 (2011) 1341–1348.
[40] P. Li, Y. Zheng, H. Ran, J. Tan, Y. Lin, Q. Zhang, J. Ren, Z. Wang, Ultrasound triggered drug release from 10-hydroxycamptothecin-loaded phospholipid microbubbles for targeted tumor therapy in mice, J. Control. Release 162 (2012) 349–354.
[41] S. Fokong, B. Theek, Z. Wu, P. Koczera, L. Appold, S. Jorge, U. Resch-Genger, M. van Zandvoort, G. Storm, F. Kiessling, T. Lammers, Image-guided, targeted and triggered drug delivery to tumors using polymer-based microbubbles, J. Control. Release 163 (2012) 75–81.
[42] C.Y. Lin, J.R. Li, H.C. Tseng, M.F. Wu, W.L. Lin, Enhancement of focused ultrasound with microbubbles on the treatments of anticancer nanodrug in mouse tumors, Nanomedicine (London) 8 (2012) 900–907.
[43] A. Ale, V. Ermolayev, E. Herzog, C. Cohrs, M.H. de Angelis, V. Ntziachristos, FMT-XCT: in vivo animal studies with hybrid fluorescence molecular tomography-X-ray computed tomography, Nat. Methods 9 (2012) 615–620.
[44] F. Gremse, B. Theek, S. Kunjachan, W. Lederle, A. Pardo, S. Barth, T. Lammers, U. Naumann, F. Kiessling, Absorption reconstruction improves biodistribution assessment of fluorescent nanoprobes using hybrid fluorescence-mediated tomography, Theranostics 4 (2014) 960–971.
[45] Y. Shi, S. Kunjachan, Z. Wu, F. Gremse, D. Moeckel, M. van Zandvoort, F. Kiessling, G. Storm, C.F. van Nostrum, W.E. Hennink, T. Lammers, Fluorophore labeling of core-crosslinked polymeric micelles for multimodal in vivo and ex vivo optical imaging, Nanomedicine (London) 10 (2015) 1111–1125.
[46] S. Fokong, M. Siepmann, Z. Liu, G. Schmitz, F. Kiessling, J. Gatjens, Advanced characterization and refinement of poly N-butyl cyanoacrylate microbubbles for ultrasound imaging, Ultrasound Med. Biol. 37 (2011) 1622–1634.
[47] S. Kunjachan, F. Gremse, B. Theek, P. Koczera, R. Pola, M. Pechar, T. Etrych, K. Ulbrich, G. Storm, F. Kiessling, T. Lammers, Noninvasive optical imaging of nanomedicine biodistribution, ACS Nano 7 (2013) 252–262.
[48] F. Gremse, D. Doleschel, S. Zafarnia, A. Babler, W. Jahnen-Dechent, T. Lammers, W. Lederle, F. Kiessling, Hybrid μCT-FMT imaging and image analysis, J. Vis. Exp. (2015).
[49] V. Ntziachristos, J. Ripoll, L.V. Wang, R. Weissleder, Looking and listening to light: the evolution of whole-body photonic imaging, Nat. Biotechnol. 23 (2005) 313–320.
[50] V. Ntziachristos, Going deeper than microscopy: the optical imaging frontier in biology, Nat. Methods 7 (2010) 603–614.
[51] S. Kunjachan, R. Pola, F. Gremse, B. Theek, J. Ehling, D. Moeckel, B. Hermanns-Sachweh, M. Pechar, K. Ulbrich, W.E. Hennink, G. Storm, W. Lederle, F. Kiessling, T. Lammers, Passive versus active tumor targeting using RGD- and NGR-modified polymeric nanomedicines, Nano Lett. 14 (2014) 972–981.
[52] T. Lammers, P. Peschke, R. Kuhnlein, V. Subr, K. Ulbrich, J. Debus, P. Huber, W. Hennink, G. Storm, Effect of radiotherapy and hyperthermia on the tumor accumulation of HPMA copolymer-based drug delivery systems, J. Control. Release 117 (2007) 333–341.
[53] N. Rapoport, A. Payne, C. Dillon, J. Shea, C. Scaife, R. Gupta, Focused ultrasound-mediated drug delivery to pancreatic cancer in a mouse model, J. Ther. Ultrasound 1 (2013) 11.
[54] P.G. Sanches, M. Muhlmeister, R. Seip, E. Kaijzel, C. Lowik, M. Bohmer, K. Tiemann, H. Grull, Ultrasound-mediated gene delivery of naked plasmid DNA in skeletal muscles: a case for bolus injections, J. Control. Release 195 (2014) 130–137.
[55] B. Theek, F. Gremse, S. Kunjachan, S. Fokong, R. Pola, M. Pechar, R. Deckers, G. Storm, J. Ehling, F. Kiessling, T. Lammers, Characterizing EPR-mediated passive drug targeting using contrast-enhanced functional ultrasound imaging, J. Control. Release 182 (2014) 83–89.
[56] S.N. Ekdawi, J.M. Stewart, M. Dunne, S. Stapleton, N. Mitsakakis, Y.N. Dou, D.A. Jaffray, C. Allen, Spatial and temporal mapping of heterogeneity in liposome uptake and microvascular distribution in an orthotopic tumor xenograft model, J. Control. Release 207 (2015) 101–111.
[57] E. Brown, T. McKee, E. diTomaso, A. Pluen, B. Seed, Y. Boucher, R.K. Jain, Dynamic imaging of collagen and its modulation in tumors in vivo using second-harmonic generation, Nat. Med. 9 (2003) 796–800.
[58] S. Kotopoulis, G. Dimcevski, O.H. Gilja, D. Hoem, M. Postema, Treatment of human pancreatic cancer using combined ultrasound, microbubbles, and gemcitabine: a clinical case study, Med. Phys. 40 (2013) 072902.